Spectrum of Light Quasi-Elastically Scattered from Suspensions of Tobacco Mosaic Virus. Experimental Study of Anisotropy in Translational Diffusion

Kenji Kubota,* Hisako Urabe, and Yasunori Tominaga

Department of Physics, Faculty of Science, Ochanomizu University, 1-1 Otsuka, 2 Chome, Bunkyo-ku, Tokyo 112, Japan

Satoru Fujime

Mitsubishi-Kasei Institute of Life Sciences, Machida, Tokyo 194, Japan.
Received November 17, 1983

ABSTRACT: Quasi-elastic light scattering experiments are reported on tobacco mosaic virus in 10^{-3} M Na_2HPO_4 buffer solution (pH 7.5). The theoretical formulation (Maeda, T.; Fujime, S. *Macromolecules* **1984**, *17*, 1157) for a thin rigid rod including anisotropy in translational diffusion was thoroughly examined by cumulant and two-exponential analyses of correlation functions. The cumulant analysis confirmed a recent result (Wilcoxon, J.; Schurr, J. M. *Biopolymers* **1983**, *22*, 849). The results of the two-exponential analysis showed a good agreement with the theory. The analyses were highly consistent with each other and elucidated a large effect of anisotropy in translational diffusion on dynamic light scattering spectra. The behaviors of correlation functions against the magnitude of the momentum transfer vector were examined, and a good agreement was obtained between experimental and theoretical correlation functions. The present results imply that both the rotational diffusion coefficient and the sideways and lengthways translational diffusion coefficients can be determined simultaneously from dynamic light scattering measurements.

Introduction

Recent progress in laser and microelectronics technology makes it possible to detect and extract valuable information on the dynamics of macromolecules in solution.[1,2] Photon correlation spectroscopy gives information of transport properties and relaxation processes as well as the molecular weights and sizes of macromolecules by the angular dependence of the scattered light intensity.

This spectroscopy has been successfully applied to various flexible polymer systems, for example polystyrene, from dilute to semidilute region and has given enormous useful results about the dynamics with newly developed theoretical works, such as the scaling concept.[3]

In a small KR_g or KL region, where K [$=(4\pi/\lambda)\sin(\theta/2)$] is the magnitude of the momentum transfer vector, λ the wavelength of light in the medium, θ the scattering angle, R_g the radius of gyration, and L the length of a rod, the first cumulant $\bar{\Gamma}$ of the dynamic structure factor gives the translational diffusion coefficient. In the region of $KR_g > 1$ or $KL > 1$, the dynamic structure factor includes information of the internal motion, the longest intramolecular relaxation time, or the rotational diffusion coefficient. In the case of semiflexible polymers, such as muscle thin filaments,[4] the bending motion of the filament is included further and the analysis of the correlation function becomes very complicated.

In this paper, we investigated the spectrum of light quasi-elastically scattered from a suspension of a thin rigid rod, tobacoo mosaic virus (TMV). Many dynamic light scattering studies on TMV have been carried out.[5-10] The results on the translational diffusion coefficient except for the latest one are quite incompatible with a sedimentation result.[11] The sedimentation result, $s^0_{20,w} = 188 \pm 1$ S, gives the translational diffusion coefficient $D^0_{20,w} = 4.24 \times 10^{-8}$ cm^2/s with the molecular weight of 40×10^6.[12] Earlier light scattering studies gave $D_{20,w} = (2.8\text{–}3.5) \times 10^{-8}$ cm^2/s. This value is quite too low compared with the value calculated from Broersma's[13] and Garcia de la Torre's[14] equations assuming a length (L) of 300 nm and a diameter (d) of 18 nm. This discrepancy of the translational diffusion coefficients from light scattering and sedimentation has already been mentioned by Fujime as a concentration dependence. He estimated $D^0_{20,w} = 4.5 \times 10^{-8}$ cm^2/s for the zero concentration limit.[8] Indeed, the latest work of Wilcoxon and Schurr[11] reported $D^0_{20,w} = (4.19 \pm 0.10) \times 10^{-8}$ cm^2/s, which is in good agreement with the sedimentation result. According to the theories of Broersma[13] and Garcia de la Torre,[14] TMV must have a fairly large anisotropy, $D_3 - D_1$, where D_3 and D_1 are the lengthways and sideways translational diffusion coefficients, respectively. Maeda and Saito first pointed out theoretically a quite large effect of anisotropy on power spectra for TMV solutions.[16] Fujime suggested that $(D_3 - D_1)/D_0$ should be about 0.6.[8] On the contrary, Schaefer et al. reported that $(D_3 - D_1)/D_0$ should be very small, or even *negative* for any reasonable value of rotational diffusion coefficient.[9] Hartford obtained a high value of D_0 ($(4.2\text{–}4.3) \times 10^{-8}$ cm^2/s at the scattering angle of 49.8°) but failed to detect the effect of anisotropy on his power spectra at higher scattering angles.[17] (Some details of these studies[8,9,17] will be reconsidered in Appendix A in the light of the present result.) On the basis of their own theory, Rallison and Leal[18] tried to observe the effect of anisotropy on experimental results of Wada et al.,[19] resulting in negligible anisotropy again. Loh et al. tried to decompose the correlation function into two exponentials.[10] They obtained $D_0 = 3.2 \times 10^{-8}$ cm^2/s from the slow decay component. The amplitude ratio of the fast-decay component to the slow-decay component was smaller than that from Pecora's theory.[20] On the basis of Gierke's theory,[21] Loh concluded that this smaller amplitude ratio came from anisotropy in translational diffusion of TMV.[22] However, Loh et al.'s results seem to be unusual in a sense that both decay rates (fast and slow) are proportional to K^2 and the amplitude ratio is almost constant at higher scattering angles.[10] Therefore, Loh's conclusion is quite indefinitive. A critique by Wilcoxon and Schurr[11] to the preparation of the solution in Loh's work is noteworthy. Recently, Wilcoxon and Schurr formulated an expression for the first cumulant of the correlation function.[11] They also measured the correlation functions of TMV (K^2 range up to ca. 20×10^{10} cm^{-2}). From the K^2 dependence of the apparent diffusion coefficient, they obtained $(D_3 - D_1)/D_0 = 0.43$ for the literature value[15] of the rotational diffusion coefficient of

0024-9297/84/2217-2096$01.50/0 © 1984 American Chemical Society

318 s^{-1}. This value for anisotropy is in agreement with the prediction of de la Torre theory. In their analysis, however, an apparent diffusion coefficient was deduced from a single-exponential fit and the comparison was not carried out on the entire time range of correlation functions with those based on a theory including the anisotropy effect. Thus, the detailed structure of the correlation function is still ambiguous and more detailed examinations are essential for the consideration of anisotropy of diffusion coefficients.

Maeda and Fujime reformulated the theory including the anisotropic translational diffusion.[23] They gave an expression for the first cumulant of the correlation function, which is essentially the same as that of Wilcoxon and Schurr although theoretical approaches were different from each other. Moreover, Maeda and Fujime derived explicitly the correlation function by using a perturbation technique (the interrelation between their theory and Gierke's exact one has been discussed in Appendix G of ref 23). On the basis of the theory, the amplitude and the decay rate of each mode can be obtained. This makes it possible to compare, in a much more detailed manner, the measured correlation function with the theoretical one. In this paper, in addition to the first cumulant analysis, the decomposition of the correlation function into two exponentials will be performed and the consistency of the parameters determined will be examined. The comparison of the profiles of the theoretical correlation function with experimental one will also be carried out. A brief summary of theoretical formulation by Maeda and Fujime[23] is described below.

Theoretical Background

Define the laboratory-fixed coordinate system (r,θ,ϕ) where the polar axis is taken to be parallel to the **K** vector. Let **R** be the position vector of the center-of-mass of the rod and **u** be the unit vector parallel to the long axis of the rod. To formulate an expression for the field correlation function of light scattered from a solution of a rigid rod, we have to have the conditional probability $G(\mathbf{R} - \mathbf{R}',\mathbf{u},\mathbf{u}';\tau)$ that if the rod is found at $\mathbf{R}'$ with orientation $\mathbf{u}'$ at time t', it will be found at **R** with orientation **u** at time t ($\tau \equiv |t - t'|$). Since we consider only polarized light scattering, an explicit form of ϕ-dependence of G is not required. Let $G_K(\xi,\xi';\tau)$ be the Fourier space transform of $G(\mathbf{R} - \mathbf{R}',\mathbf{u},\mathbf{u}';\tau)$ and define

$$D_0 = (2D_1 + D_3)/3 \quad \text{(the average diffusion coefficient)} \tag{1a}$$

$$\mu^2 = (D_3 - D_1)K^2/\Theta \quad \text{(the coupling constant)} \tag{1b}$$

$$G_K(\xi,\xi';\tau) = G_D(\tau)g_K(\xi,\xi';\tau) \tag{1c}$$

$$G_D(\tau) = \exp[-\{D - \tfrac{1}{3}(D_3 - D_1)\}K^2\tau] \equiv \exp[-D_1K^2\tau] \tag{1d}$$

$g_K(\xi,\xi';\tau)$ satisfies the diffusion equation

$$[\partial/\partial\tau - \Theta(\nabla_\xi{}^2 - \mu^2\xi^2)]g_K(\xi,\xi';\tau) = \delta(\xi - \xi')\delta(\tau) \tag{2}$$

where Θ is the rotational diffusion coefficient, $\xi = \cos\theta$, θ being the angle between **u** and **K**, and $\nabla_\xi{}^2$ is the Laplace operator. Due to nonzero values of μ^2 for a long rod, rotational diffusion is not independent of translational diffusion. By expanding $g_K(\xi,\xi';\tau)$ in terms of the Legendre polynomial $P_n(\xi)$, substituting it into eq 2, multiplying both sides by $P_n(\xi)$, and integrating over ξ, we have simultaneous first-order differential equations for expansion coefficients $A_n(K,\xi',\tau)$, which can be written in a matrix form as

$$\partial\mathbf{A}/\partial(\Theta\tau) = -\mathbf{MA} \tag{3}$$

where $\mathbf{A} = [A_0, A_2, A_4, ..., A_N]^t$ (t means transposition and A_n was truncated at $n = N$) and $\mathbf{M} = \{a_{n,m}\}$ with

$$a_{n,n} = n(n+1) + \mu^2L_0(n)$$
$$a_{n,n-2} = \mu^2L_1(n) \tag{4}$$
$$a_{n,n+2} = \mu^2L_2(n)$$

and $a_{n,m} = 0$ for $m \neq n$ and $n \pm 2$. $L_i(n)$ ($i = 0$, 1, and 2) are given by

$$L_0(n) = (2n^2 + 2n - 1)/(2n - 1)(2n + 3)$$
$$L_1(n) = n(n - 1)/(2n - 1)(2n - 3) \tag{5}$$
$$L_2(n) = (n + 1)(n + 2)/(2n + 3)(2n + 5)$$

Once the matrix is diagonalized, eq 3 can be solved easily and we have the solution of eq 2. For this, we have to solve the eigenvalue problem:

$$\mathbf{MU}_p = \lambda_p\mathbf{U}_p \quad \text{and} \quad \mathbf{U}_p{}^*\mathbf{M} = \lambda_p\mathbf{U}_p{}^* \tag{6}$$

where λ_p is the eigenvalue of **M**, $\mathbf{U}_p = [U_p(0), U_p(2), U_p(4), ..., U_p(N)]^t$ is the column eigenvector of **M**, and $\mathbf{U}_p{}^* = [U_p{}^*(0), U_p{}^*(2), U_p{}^*(4), ..., U_p{}^*(N)]$ is the line eigenvector of **M**. Using these results, we have the field correlation function in the form

$$G^{(1)}(\tau) = G_D(\tau)\sum_p\sum_n\sum_m(2m + 1) \times U_p(n)U_p{}^*(m)i^{n+m}b_n(k)b_m(k)\exp(-\lambda_p\Theta\tau) \tag{7}$$

where summations are carried out over even m, n, and p, $k \equiv KL/2$, and

$$b_n(k) = \frac{1}{k}\int_0^k j_n(z)\,dz \quad \text{for even } n$$
$$= 0 \quad \text{for odd } n \tag{8}$$

The function $j_n(z)$ is the nth-order spherical Bessel function. In the case of $\mu = 0$, that is, $D_3 - D_1 \ll 1$ and/or $KL \ll 1$, eq 7 is reduced to Pecora's formula for the rod undergoing isotropic translational diffusion:[20]

$$G^{(1)}(\tau) = \sum_n S_n(k)\exp[-\{D_0K^2 + n(n+1)\Theta\}\tau] \tag{9}$$

$$S_n(k) = (2n + 1)b_n(k)^2 \tag{10}$$

Without solving eq 6, the first cumulant $\bar{\Gamma}$ of $G^{(1)}(\tau)$ can be known:

$$\bar{\Gamma}/K^2 = [D_0 - \tfrac{1}{3}(D_3 - D_1)] + (L^2/12)\Theta f_1(k) + (D_3 - D_1)f_2(k) \tag{11}$$

where both $f_1(k)$ and $f_2(k)$ are functions depending only on k.

To solve eq 6 for $\mu^2 \leq 6$, a perturbation technique can be applied. Divide **M** into two parts, $\mathbf{M} = \mathbf{M}^{(0)} + \epsilon\mathbf{M}^{(1)}$, where $\mathbf{M}^{(0)}$ consists of only the diagonal elements of **M**, $\mathbf{M}^{(1)}$ consists of only the off-diagonal elements of **M**, and ϵ is a perturbation parameter that is set to unity eventually. The perturbation results to first order in ϵ are easily obtained, and substitution of them into eq 7 gives

$$G^{(1)}(\tau) = G_D(\tau)\sum_{\text{even } n}\left[S_n(k)\exp(-\lambda_n\Theta\tau) - 2(2n + 5) \times b_n(k)b_{n+2}(k)\mu^2L_2(n)\frac{\exp(-\lambda_n\Theta\tau) - \exp(-\lambda_{n+2}\Theta\tau)}{\lambda_n - \lambda_{n+2}}\right] \tag{12a}$$

$$= P_0(k)\exp(-\Gamma_0\tau) + P_2(k)\exp(-\Gamma_2\tau) + P_4(k)\exp(-\Gamma_4\tau) + ... \tag{12b}$$

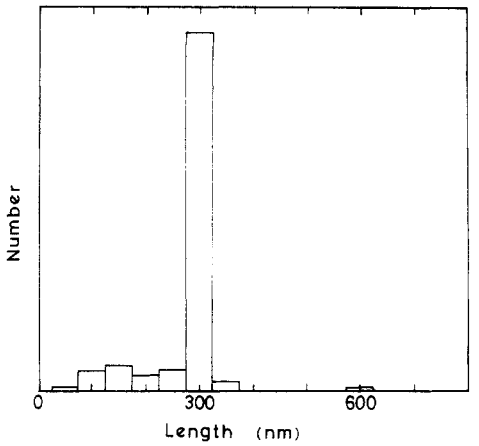

Figure 1. Length distribution of tobacco mosaic virus used for the experiments. From electron micrographs.

where $\lambda_n = n(n+1) + \mu^2 L_0(n)$. Because $\mathbf{M}^{(1)}$ lacks its diagonal elements, it does not contribute to λ_n's to order ϵ. From the results in Appendix B, we have Γ_0 and Γ_2 to order ϵ^2:

$$\Gamma_0 = D_0K^2 - A_0(\mu^2)[(D_3 - D_1)^2/\Theta]K^4 \quad (12c)$$

$$\Gamma_2 = D_0K^2 + (4/21)(D_3 - D_1)K^2 + 6\Theta + [A_0(\mu^2) - A_2(\mu^2)][(D_3 - D_1)^2/\Theta]K^4 \quad (12d)$$

These results predict that Γ_0/K^2 $[(\Gamma_2 - \Gamma_0)/6]$ has a negative [positive] slope against K^2 (see Figures 5 and 6). There is a typographic error in ref 18; i.e., their Γ_0 should read $[\bar{D}(ql)^2 - \bar{D}'^2(ql)^4/30 + ...]D$. By numerically solving the eigenvalues λ_p of the matrix $\mathbf{M}$ and substituting them into eq 12, we can construct a better correlation function than that from pure perturbation results. In case of TMV for $K^2 \leq 11 \times 10^{10}$ cm^{-2}, μ^2 is not more than 8. Therefore, the matrix with 4×4 elements is large enough to obtain accurate λ_p's.

Experimental Section

1. Tobacco Mosaic Virus. TMV samples used in this study were kindly provided by Dr. Kubo of the Central Research Institute, the Japan Tobacco and Salt Public Corp. The original concentration of this TMV suspension was approximately 42 mg/mL. A part of this suspension (stored at −80 °C) was first diluted by 400 times in 10^{-3} M Na_2HPO_4 buffer (pH 7.5) and the concentration of this solution was determined from the absorbance at 260 nm by using a Shimazu UV-120-02 spectrophotometer. The absorbance was 0.144 for 5-mm light path and the concentration was determined to be 0.096 mg/mL according to the value of the extinction coefficient 3.0 for 1 mg/mL and 1-cm light path.[24] The solution was further diluted to the concentration for the measurements and stored at −10 °C until use. All the measurements were carried out within 2–3 days after the final dilution. The TMV solution was filtered through a Millipore filter with 0.45-μm pore size directly into the scattering cell, which was a 10-mm-o.d. polished cylindrical cell and was thoroughly rinsed with the same buffer solution.

Polydispersity of the TMV sample was checked by electron microscopy. Almost all the images on micrographs showed single, perfect TMV particles with length 300 nm. The length distribution determined from micrographs is shown in Figure 1. From the total scattering intensity, we obtained R_g = 85.6 nm, or L = 297 nm from $L = 12^{1/2}R_g$, which again confirms the quality of samples.

2. Light Scattering. The light scattering measurements were made with a homemade spectrometer and a 252-channel real-time digital correlator.[25] The diagram of the apparatus is shown in Figure 2. We used an argon ion laser (GLG-3200, NEC, Japan) operating at 488.0 nm. The temperature was held constant at 25.6 ± 0.05 °C. The scattering angle ranged from 27.5° to 150°, covering $K^2 = (0.66–11) \times 10^{10}$ cm^{-2}. The scattered intensity was

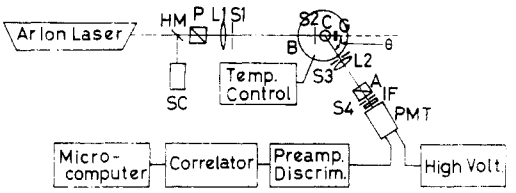

Figure 2. Schematic diagram of the experimental arrangement. L_1 and L_2, lenses; S_1–S_4, pin holes; P, polarizer; A, analyzer; C, sample cell; G, absorbing neutral-density filter; B, heat bath with index-matching oil; HM, half-mirror; SC, solar cell for monitoring the incident beam intensity; PMT, photomultiplier tube; IF, interference filter; θ, scattering angle.

monitored by a frequency counter in order to check dusts and large aggregates, and the count rate was satisfactorily constant.

The light scattering spectrometer was calibrated by use of standard samples, i.e., benzene, toluene, and polystyrene latex with diameter 91 nm. The scattered intensity from benzene and toluene was constant after the scattering volume correction, within 1% from 25° to 150°, and within less than 3% from 15° to 25°. The first cumulant observed for a polystyrene latex suspension (ca. 10^{-5} g/g) was in quite good agreement (within 1%) with the value from the diameter of 91 nm. For a test of the correlator, the correlation function of the intensity of light from a lamp powered by a stabilized dc voltage source was measured. Such correlation functions should be flat in delay times, and the measured ones were indeed quite constant over all channels. The correlator was of the clipping type with one-bit (binary digit) shift registers as delaying components.[25] This equipped a circuit to determine the background or base line, that is, 12 additional channels starting from the 2048th channel after the 240th channel. Final accumulation of the correlation function was transferred to a homemade microcomputer (8-bit CPU) and data analysis was carried out after each measurement.

3. Data Analysis. The measured intensity autocorrelation function, $Y(\tau)$, in the homodyne mode is related to the normalized field correlation function $g^{(1)}(\tau)$, which is given by $G^{(1)}(\tau)/G^{(1)}(0)$ in eq 7, as

$$Y(\tau) = B[1 + \beta|g^{(1)}(\tau)|^2] \quad (13)$$

where B is the base line and β is a machine constant. Measured correlation functions were first fitted to the equations

$$Y(\tau) = P \exp[-2\bar{\Gamma}\tau + 2(\mu_2/2!)\tau^2 - ...] + B \quad (14)$$

and

$$Y(\tau) = R \exp(-\tau/\tau_c) + B \quad (15)$$

Equation 14 is a cumulant expansion[26] and $\bar{\Gamma}$ is the average decay rate or the first cumulant; μ_2 is the second cumulant and $\mu_2/\bar{\Gamma}^2$ gives the normalized dispersion. Equation 15 is also used after the method of Schurr et al.[11] An apparent decay rate, corresponding to $\bar{\Gamma}$ in eq 14, is given by $(2\tau_c)^{-1}$.

Goodness of the data fitting was monitored in several points. The fitted base line should not differ from the measured one by more than 0.5%.[27] The square of deviation of the fitted function from the measured one normalized by the variance of the measured one should be reasonably small, and the standard deviation of parameters determined should be less than 10%. Also, the deviation of the fitted function from the measured one should be reasonably random. This is checked by the equation

$$Q = 1 - \sum_I [Y_m(I) - Y_c(I)][Y_m(I+1) - Y_c(I+1)] / \sum_I Y_m(I)^2 \quad (16)$$

where $Y_m(I)$ is the value of the Ith experimental point and $Y_c(I)$ is the value of the Ith calculated point of the correlation function. Q should not be smaller than 0.5, because a systematic deviation is observed when Q is smaller than 0.5. In all measurements, the sampling time ($\Delta\tau$) for each channel or the channel delay time was chosen so that the total delay time, $240\Delta\tau$, was about $3/\bar{\Gamma}$ in order to ensure a high quality of data analysis.

As seen from eq 12, for the thin rod at large KL, the correlation function $G^{(1)}(\tau)$ is expressed by two exponential components or

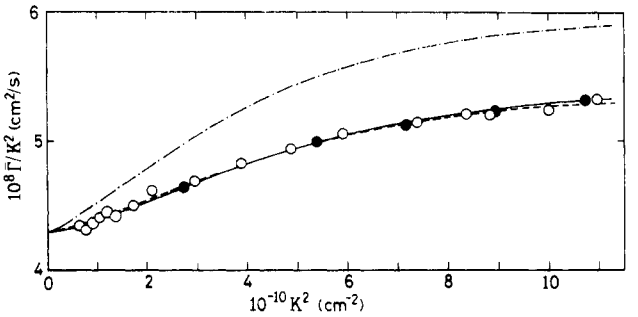

Figure 3. $\bar{\Gamma}/K^2$ vs. K^2 relationship corrected to 20 °C in water. The solid and dashed lines denote the reconstructed theoretical curves with $D_0 = 4.29 \times 10^{-8}$ cm^2/s, $\Theta = 320$ s^{-1}, $(D_3 - D_1)/D_0 = 0.500$, and $L = 300$ nm and with $D_0 = 4.30 \times 10^{-8}$ cm^2/s, $\Theta = 295$ s^{-1}, $(D_3 - D_1)/D_0 = 0.412$, and $L = 300$ nm, respectively (see text). The dot–dash line denotes the reconstructed theoretical curve for the isotropic case with $D_0 = 4.29 \times 10^{-8}$ cm^2/s and $\Theta = 320$ s^{-1}. Filled circles show the results from the two-exponential fit for the generated correlation functions with the same parameter values for the solid line (see text).

more. Therefore, the measured correlation function was fitted to

$$Y(\tau) = [A_0 \exp(-\Gamma_0\tau) + A_2 \exp(-\Gamma_2\tau)]^2 + B \qquad (17)$$

where Γ_0 (slow decay mode) and Γ_2 (fast decay mode) are the decay rates with amplitudes A_0 and A_2, respectively. As stated in the previous section, Γ_0 corresponds essentially to translational diffusion and Γ_2 corresponds to the coupling of the translational and rotational diffusion. Roughly speaking, Γ_0/K^2 gives the average translational diffusion coefficient D_0 and $(\Gamma_2 - \Gamma_0)/6$ gives the rotational diffusion coefficient Θ [*plus* an additional term $(2/63)(D_3 - D_1)K^2$]. The behavior of Γ_0, $(\Gamma_2 - \Gamma_0)$, and A_2/A_0 against KL or K^2 can be predicted by the theory. From the decomposition of experimental correlation functions into two exponentials, consistency of obtained molecular parameters can be thoroughly examined.

Results

We measured the intensity autocorrelation function $Y(\tau)$ of scattered light from suspensions at 0.02 and 0.06 mg/mL TMV over the K^2 range $(0.66–11) \times 10^{10}$ cm^{-2}. The experimental $Y(\tau)$ was analyzed mainly by the two methods mentioned in the preceding section.

1. Cumulant Analysis. The second-order cumulant analysis was first carried out. The $\bar{\Gamma}/K^2$ vs. K^2 relationship is shown in Figure 3. This relationship was the same within experimental error for the two concentrations studied, and no correction was made. The normalized dispersion $\mu_2/\bar{\Gamma}^2$ was generally less than 0.1. The relative deviation of the base line was also generally less than 0.2%. The correlation coefficients Q in eq 16 were large (0.6–0.8) enough to prove that the fitting was good. For comparison with the previous studies, the single-exponential analysis was also carried out. The resultant values for $(2\tau_c K^2)^{-1}$ over all K^2 values studied were slightly smaller than the corresponding $\bar{\Gamma}/K^2$ values, but the overall profile of the $(2\tau_c K^2)^{-1}$ vs. K^2 relationship was quite similar to that of $\bar{\Gamma}/K^2$. However, the correlation coefficients Q were usually much smaller and less than 0.5 for all the measured $Y(\tau)$'s. Since systematic deviations were clearly present, we did not use the $(2\tau_c K^2)^{-1}$ vs. K^2 relationship for further examinations.

The average translational diffusion coefficient D_0 was determined from the $\bar{\Gamma}$ vs. K^2 relationship at small K^2 values and was obtained to be $(4.30 \pm 0.10) \times 10^{-8}$ cm^2/s. The length L of TMV was determined from electron micrographs to be 300 nm. Then all of the data of $\bar{\Gamma}/K^2$ as a function of K^2 were analyzed by use of eq 11. For this purpose, the numerical values of $f_1(k)$ and $f_2(k)$ were obtained from the tabulated values in ref 23, where a spline subroutine was used for interpolation. Figure 4 illustrates $f_1(k)$ and $[1/3 - f_2(k)]$ as a function of K^2. For $D_0 = (4.30 \pm 0.10) \times 10^{-8}$ cm^2/s and $L = 300$ nm, the least-squares fit gave $\Theta = 295$ s^{-1} and $(D_3 - D_1)/D_0 = 0.412$. For the same value of L and $\Theta = 320$ s^{-1} from a two-exponential fit given later, the least-squares fit gave $D_0 = 4.29 \times 10^{-8}$ cm^2/s and $(D_3 - D_1)/D_0 = 0.500$. Table I lists our results, where the italicized figure(s) was given in the least-squares analysis. From this table, we can find a systematic trend. The D_0 value is insensitive to the initial condition(s) (or constraint(s)) in the analysis, whereas Θ and $(D_3 - D_1)/D_0$ change in a correlated way; i.e., the larger the Θ value, the larger the $(D_3 - D_1)$ value. This is a natural consequence of the functional form of eq 11. Equation 11 can be written in the form

$$\bar{\Gamma}/K^2 = D_0 - (D_3 - D_1)[1/3 - f_2(k)] + (L^2/12)\Theta f_1(k) \qquad (18)$$

where D_0 is the "base line" and the functions $[1/3 - f_2(k)]$ and $f_1(k)$ behave in a similar way (see Figure 4), i.e., starting from zero at $K^2 = 0$, increasing monotonically with K^2, and reaching individual final values at large K^2. A larger "given" value of Θ results in a larger value of $(D_3 - D_1)$ and vice versa (see Discussion). Using obtained values of D_0, Θ, and $(D_3 - D_1)/D_0$, the $\bar{\Gamma}/K^2$ vs. K^2 relationship was reconstructed. The dashed line in Figure 3 is from the parameter values in the first line in Table I, and the solid line from those in the second line. Both are in good agreement with experimental points. The experimental result is completely different from the theoretical prediction (the dash–dot line in Figure 3) in the absence of anisotropy in translational diffusion.

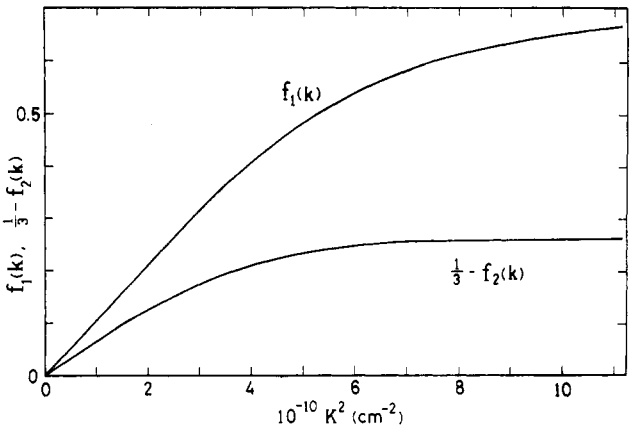

Figure 4. Graphic representation of $f_1(k)$ and $(1/3 - f_2(k))$ as a function of K^2 for $L = 300$ nm.

Table I
Results of the First Cumulant Analysis for $L = 300$ nm[a,b]

$D_0 \times 10^8$, cm^2/s	Θ, s^{-1}	$(D_3 - D_1)/D_0$
4.30	295	0.412
4.29	*320*[c]	0.500
4.30	*320*	0.510
4.29	*295*	0.397
4.23	230	0.087

[a] Representative standard deviations are 0.10 in D_0, 30 in Θ, and 0.100 in $(D_3 - D_1)/D_0$. [b] Italicized figure(s) was given in the least-squares fit. [c] From the two-exponential analysis.

2. Two-Exponential Analysis. At low angles, the two-exponential analysis did not give any definitive result because of the smallness of the ratio A_2/A_0. Therefore, we carried out the analysis for $Y(\tau)$'s at $\theta \geq 60°$. The results Γ_0/K^2 and $(\Gamma_2 - \Gamma_0)/6$, both corrected to 20 °C in water, and A_2/A_0 are shown in Figures 5–7, respectively. The Γ_0/K^2 $[(\Gamma_2 - \Gamma_0)/6]$ first decreases [increases] linearly

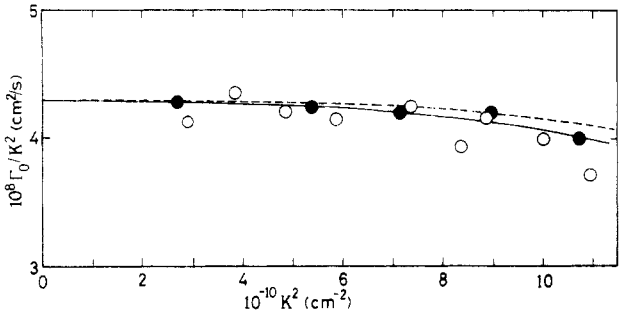

Figure 5. Γ_0/K^2 vs. K^2 relationship. The Γ_0 was obtained from the slow-decay component of the two-exponential fit and is corrected to 20 °C in water. Other notations are the same as those in Figure 3.

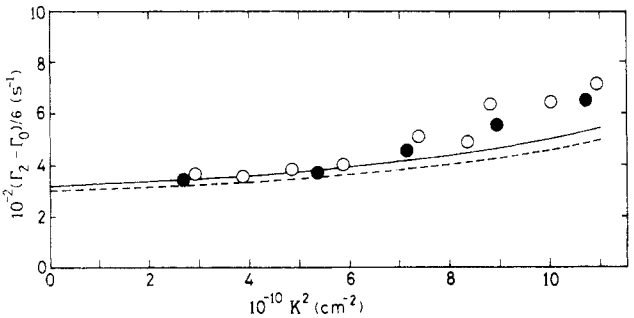

Figure 6. $(\Gamma_2 - \Gamma_0)/6$ vs. K^2 relationship. Γ_2 and Γ_0 are the fast- and slow-decay rates of the two-exponential fit and are corrected to 20 °C in water. Other notations are the same as those in Figure 3.

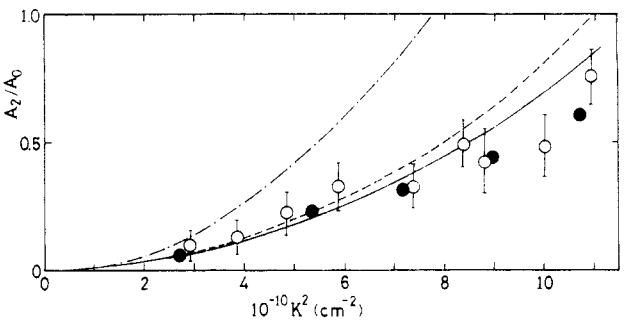

Figure 7. Ratio of the amplitudes of the two-exponential fit as a function of K^2. A_0 and A_2 are the amplitudes of the slow- and fast-decay components. Other notations are the same as those in Figure 3.

with K^2 and then a little bit rapidly. These behaviors are compatible with theoretical results in eq 12c,d but quite incompatible with the theory for the case of isotropic translational diffusion. Also, our result for Γ_2 is quite different from that of Loh et al.[20] The amplitude ratio A_2/A_0 is also very incompatible with $S_2(k)/S_0(k)$ or $[S_2(k) + S_4(k)]/S_0(k)$ in eq 10, the dash-dot line in Figure 7.

According to the theory given in the previous section, the extrapolation to $K^2 = 0$ of Γ_0/K^2 and $(\Gamma_2 - \Gamma_0)/6$ deduced from the two-exponential fit should give D_0 and Θ, respectively. The extrapolated values are $D_0 = (4.2\text{–}4.3) \times 10^{-8}$ cm²/s in Figure 5 and $\Theta = 320$ s⁻¹ in Figure 6. Both are in good agreement with those from the analysis of $\bar{\Gamma}/K^2$ given before. Although we could observe the K^2 dependence of $(\Gamma_2 - \Gamma_0)/6$ in Figure 6, it would be difficult to determine precisely the $(D_3 - D_1)$ value from $(\Gamma_2 - \Gamma_0)/6 = \Theta + (2/63)(D_3 - D_1)K^2 + \ldots$ as Gierke has proposed[21] and Hartford had tried.[17]

For large K^2 values, say $K^2 > 6 \times 10^{10}$ cm⁻², both Γ_0/K^2 and $(\Gamma_2 - \Gamma_0)/6$ deviate from the first-order perturbation results; i.e., Γ_0/K^2 is independent of K^2 and $(\Gamma_2 - \Gamma_0)/6 - \Theta$ depends linearly on K^2. Then theoretical evaluation

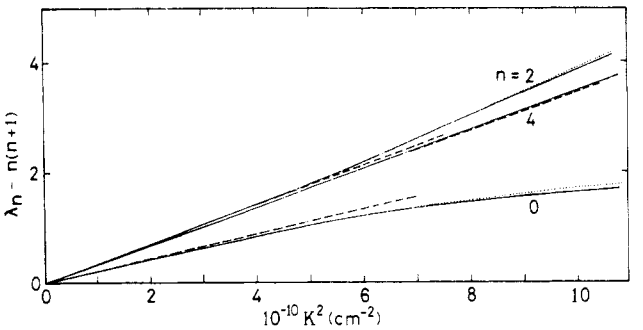

Figure 8. Eigenvalues of the 4 × 4 matrix **M** for $D_0 = 4.29 \times 10^{-8}$ cm²/s, $\Theta = 320$ s⁻¹, and $(D_3 - D_1)/D_0 = 0.500$. The zeroth-order perturbation results (dashed lines) are expressed as $(1/3)(D_3 - D_1)K^2/\Theta$, $(11/21)(D_3 - D_1)K^2/\Theta$, and $(39/77)(D_3 - D_1)K^2/\Theta$ for $n = 0$, 2, and 4, respectively. The dotted lines show the second-order perturbation results for $n = 0$ and 2. For $n = 4$, the dotted line overlaps with the solid line within its width.

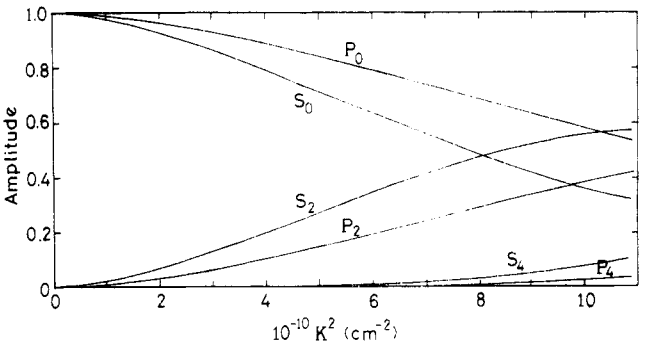

Figure 9. Theoretical amplitudes $P_n(k)$ in eq 12b as a function of K^2 for $D_0 = 4.29 \times 10^{-8}$ cm²/s, $\Theta = 320$ s⁻¹, $(D_3 - D_1)/D_0 = 0.500$, and $L = 300$ nm. The theoretical amplitudes $S_n(k)$ in eq 10 (Pecora's S_n) are also shown for comparison. Note that P_n and S_n are plotted in a normalized manner as $\sum P_n = \sum S_n = 1$ for each K^2 value.

was carried out in the following way. For example, using $D_0 = 4.29 \times 10^{-8}$ cm²/s, $\Theta = 320$ s⁻¹, and $(D_3 - D_1)/D_0 = 0.500$, we constructed the matrix **M** for various values of K^2 or μ^2. Theoretical values of λ_n's for the 4 × 4 matrix are shown in Figure 8. By using these rigorous values of λ_n's, we computed $P_n(k)$ in eq 12b for $n = 0$, 2, and 4. Even when rigorous eigenvectors of the 4 × 4 matrix were used, the computed $P_n(k)$'s were almost the same as those from the first-order perturbation results for the present range of K^2. For example, at $K^2 = 8.95 \times 10^{10}$ cm⁻² or $\mu^2 = 6.0$, the 4 × 4 matrix yielded $\lambda_0 = 1.5712$ (2.0), $\lambda_2 = 9.4019$ (9.1428), $\lambda_4 = 23.1048$ (23.0389), and $\lambda_6 = 45.1221$ (45.0182), where the numbers in the parentheses were from the zeroth-order result $\lambda_n = n(n + 1) + \mu^2 L_0(n)$. Substitution of these rigorous λ_n's into eq 12 yielded $P_0 = 0.6366$, $P_2 = 0.3318$, and $P_4 = 0.0211$. On the other hand, substitution of rigorous eigenvectors into eq 7 gave $P_0 = 0.6408$, $P_2 = 0.3357$, and $P_4 = 0.0234$. The differences were 0.67% for P_0, 1.17% for P_2, and 10.8% for P_4. Because of the small value of P_4, the correlation functions composed of these two sets of P_n's were indistinguishable from each other. In Figure 9, the behaviors of $P_n(k)$'s against K^2 are shown together with $S_n(k)$'s in eq 10. In the present range of K^2, P_0 is larger than S_0, whereas P_2 and P_4 are smaller than S_2 and S_4, respectively. The theoretical correlation functions were generated by using parameters obtained above. The simulated correlation functions *plus* 0.1% random noise for each channel were analyzed by the two-exponential decomposition. Results are shown by filled circles in Figures 3 and 5–7. For $\bar{\Gamma}/K^2$, a relationship $\bar{\Gamma} = (A_0\Gamma_0 + A_2\Gamma_2)/(A_0 + A_2)$ was assumed. We find a surprising agreement between experimental and

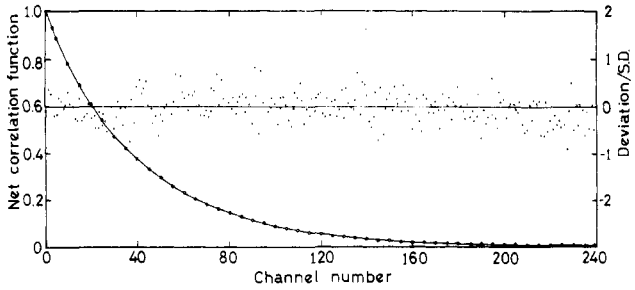

Figure 10. Net correlation function at $\theta = 120°$ as a function of channel number. Only every fifth point is displayed to avoid the cluttering. Sampling time ($\Delta\tau$) = 2.3 μs. The solid line shows the fitted curve which is based on the theoretical predictions on Γ_n's and P_n's (see text). The dots denote the deviations normalized by the standard deviation (SD) defined by $Y(\tau)^{1/2}$.

"theoretical" points. From the theoretical results, we also constructed $\Gamma_0 = [D_0 - (1/3)(D_3 - D_1)]K^2 + \lambda_0\Theta$, $\Gamma_2 = [D_0 - (1/3)(D_3 - D_1)]K^2 + (P_2\lambda_2 + P_4\lambda_4)\Theta/(P_2 + P_4)$ and $A_2/A_0 = (P_2 + P_4)/P_0$, where renormalization was assumed for Γ_2 and A_2 in order to keep consistency with the results of the two-exponential analysis. The theoretical curves for Γ_0/K^2, $(\Gamma_2 - \Gamma_0)/6$, and A_2/A_0 thus determined are shown by solid lines in Figures 5–7. The same quantities for another combination of diffusion coefficients, i.e., $D_0 = 4.30 \times 10^{-8}$ cm^2/s, $\Theta = 295$ s^{-1}, and $(D_3 - D_1)/D_0 = 0.412$, are also shown by dashed lines in these figures. The overall trend against K^2 of the theoretical curves for Γ_0/K^2, $(\Gamma_2 - \Gamma_0)/6$, and A_2/A_0 are in quite good agreement with those of measured and theoretical points. For the two sets of parameters considered above, the case of $\Theta = 320$ s^{-1} is generally better than the case of $\Theta = 295$ s^{-1}.

3. Further Analysis of Correlation Functions. The theoretical curves of Γ_0/K^2 for $\Theta = 320$ s^{-1} are in good agreement with experimental and theoretical points. For $(\Gamma_2 - \Gamma_0)/6$ and A_2/A_0, on the other hand, discrepancies between the theoretical curves and the experimental and theoretical points become conspicuous at large K^2 values. This probably implies that the assumed renormalization, $(P_2\lambda_2 + P_4\lambda_4)\Theta/(P_2 + P_4)$ in Γ_2 and $A_2 = P_2 + P_4$, is not very appropriate. Then for large K^2 values, we tried to fit the three-exponential expression

$$Y(\tau) = [A_0 \exp(-\Gamma_0\tau) + A_2 \exp(-\Gamma_2\tau) + A_4 \exp(-\Gamma_4\tau)]^2 + B \quad (19)$$

Since the seven-parameter analysis including B was not practical, we adopted an approximate method; that is, Γ_n's or A_n's were fixed to the theoretical values mentioned before (for the case of $\Theta = 320$ s^{-1}). For example, at $\theta = 120°$ or $K^2 = 8.80 \times 10^{10}$ cm^{-2}, the theoretical values were $\Gamma_0 = 3655$, $\Gamma_2 = 6140$, and $\Gamma_4 = 10530$ s^{-1} at 20 °C, and $P_0 = 0.647$, $P_2 = 0.332$, and $P_4 = 0.021$. For fixed Γ_n's to the theoretical values, the least-squares fitting of eq 19 to experimental correlation functions yielded $A_0 = 0.656$ (relative error from the theoretical value of +1.4%), $A_2 = 0.330$ (−0.6%), and $A_4 = 0.014$ (−33%). Here, A_n's are normalized as $\sum A_n = 1.0$. The deviation of the fitted base line was 0.18% from the measured base line. Although the relative error for A_4 was large, the absolute value was so small that the deviation was not so important. Actually, the correlation coefficient Q was 0.833 and large enough. The value of $(A_2 + A_4)/A_0 = 0.535$ should be compared with the theoretical value of 0.558 (−2.1%) and 0.42 determined from the two-exponential analysis. The measured and theoretical correlation functions are shown in Figure 10, where deviation at each channel of the theoretical correlation function from the measured one normalized by $Y(\tau)^{1/2}$ is also shown. Deviation is small and not systematic. When A_n's were fixed to the theoretical values, the least-squares fit yielded $\Gamma_0 = 3572$ (−2.1%), $\Gamma_2 = 6129$ (−0.2%), and $\Gamma_4 = 24\,880$ s^{-1} (136%). Except for Γ_4, both Γ_0 and Γ_2 were well reproduced.

From the analysis given above, it is shown that eq 7 and 12 reproduce measured quantities very well and that the behaviors of $\bar{\Gamma}/K^2$, Γ_0, Γ_2, and A_2/A_0 against K^2 are consistent with each other. The deviation of experimental and theoretical values for $(\Gamma_2 - \Gamma_0)/6$ and A_2/A_0 at large K^2 from theoretical curves can be explained by the artifact due to the two-exponential "force" fit. Inclusion of the effect of anisotropy in translational diffusion can explain the time behavior of correlation functions at different values of K^2 and the K^2 dependence of the parameters.

Discussion

The present value of the average diffusion coefficient, $D_0 = 4.29 \times 10^{-8}$ cm^2/s, is substantially higher than the previous results and in good agreement with that of Wilcoxon and Schurr.[11] Earlier works were usually performed at relatively high concentrations, ≥0.2 mg/mL TMV. The interparticle distance even at 0.2 mg/mL is almost the same as the particle length of TMV.[8] Brownian motions of TMV carrying a large amount of charge will be affected by the interparticle correlation, and this may cause the decrease in the value of the average diffusion coefficient. In spite of the low D_0 values, however, earlier studies gave high Θ values, 320–360 s^{-1}. It is worthwhile to reinvestigate TMV suspensions at concentrations up to 1 mg/mL with modern techniques both in the measurements and in the analysis.

In contrast to most of the previous studies, the present result as well as that of Wilcoxon and Schurr clearly indicates the large effect of anisotropy in translational diffusion on dynamic light scattering spectra. In light of the present result, we reconsidered in Appendix A some of previous studies which intended to see the effect of the anisotropy. None of them, however, could give a very quantitative result. The present success in quantitative observation of a large effect of anisotropy came primarily from a great increase in the accuracy of measured spectra by photon-counting spectroscopy and the cumulant analysis of correlation functions. In addition to this, success in quantitative analysis of the line profile of observed correlation functions came from a theoretical expression in eq 12b. Application of a standard perturbation technique to diagonalize the matrix **M** in eq 3 (and not to solve eq 3 itself) made the theoretical expression of the field correlation function very concise compared with those in the previous ones.[9,16,18]

Our analysis of the $\bar{\Gamma}/K^2$ vs. K^2 relationship was a little different from the analysis of Wilcoxon and Schurr for the $(2\tau_c K^2)^{-1}$ vs. K^2 relationship. They used a "literature" value (and a value from another of their experiments) for Θ to obtain the best fit value of $(D_3 - D_1)/D_0$. Furthermore, they made a correction to the systematic error due to the single-exponential fit, and this would introduce unnecessary ambiguity in the result. In fact, their 2% correction to $D_{app}(k) \equiv (2\tau_c K^2)^{-1}$ at $K^2 = 20 \times 10^{10}$ cm^{-2} caused more than 20% change in the anisotropy ratio. Thus the consistency of determined parameters themselves is not clear, and some degree of arbitrariness in the determined parameters will remain. In the present analysis, however, everything was carried out within our own data. The consistency of the determined parameters, D_0, Θ, and $(D_3 - D_1)/D_0$, from the least-squares fit of the $\bar{\Gamma}/K^2$ vs. K^2 relationship was proved by a further analysis of the two-exponential decomposition of correlation functions.

Table II
Comparison of the Present Result with Others (20 °C)

parameter	present	Schurr[11]	Cummins[6]	Fujime[8]	Schaefer[9]	Garcia de la Torre[14]	Broersma[28]
$10^8 D_0$, cm²/s	4.29 ± 0.10	4.19 ± 0.10	2.80	3.5	3.41 ± 0.10[c]	4.53	4.09
				4.5[a]	*3.41 ± 0.07*[d]		
Θ, s^{-1}	312 ± 30	(318)	320 ± 18	360	(366)	316	299
				390	*(366)*		
$(D_3 - D_1)/D_0$	0.474 ± 0.100	0.43 ± 0.09		0.6[b]	0.025 ± 0.12	0.394	0.308
					0.137 ± 0.073		
$10^8 D_3$, cm²/s	5.64 ± 0.29	5.38 ± 0.27				5.72	4.93
$10^8 D_1$, cm²/s	3.61 ± 0.14	3.59 ± 0.16				3.93	3.67

[a] Estimated value at infinite dilution. [b] Estimated value (see Appendix A). [c] Corrected to 20 °C. [d] The figures in italics are from our reanalysis (see Appendix A).

Here we would like to add a few comments on the least-squares analysis of the $\bar{\Gamma}/K^2$ vs. K^2 relationship. For a given Θ value, we have

$$F_1(k) \equiv \bar{\Gamma}/K^2 - (L^2/12)\Theta f_1(k) = D_0 - (D_3 - D_1)[1/3 - f_2(k)] \quad (20)$$

The K^2 dependence of $F_1(k)$ is determined solely by the K^2 dependence of $[1/3 - f_2(k)]$, so that both D_0 and $(D_3 - D_1)$ will be determined with a high accuracy. For a given D_0 value, we have

$$F_2(k) \equiv \bar{\Gamma}/K^2 - D_0 = -(D_3 - D_1)[1/3 - f_2(k)] + (L^2/12)\Theta f_1(k) \quad (21)$$

The data points at low K^2 values determine only a linear combination of $(D_3 - D_1)$ and Θ, i.e., $-(D_3 - D_1)(KL)^2/(3 \times 45) + (L^2/12)\Theta(KL)^2/(2 \times 45)$, because $[1/3 - f_2(k)] = (KL)^2/(3 \times 45) + \ldots$ and $f_1(k) = (KL)^2/(2 \times 45) + \ldots$. At high K^2 values, $[1/3 - f_2(k)]$ changes very slowly with K^2 compared with $f_1(k)$ (see Figure 4). In addition to this, the relative size of $(D_3 - D_1)[1/3 - f_2(k)]$ is less than half of $(L^2/12)\Theta f_1(k)$ for, say, $(D_3 - D_1) \simeq 2.1 \times 10^{-8}$ cm²/s and $\Theta \simeq 320$ s^{-1}. For a determination of $(D_3 - D_1)$ and Θ values with high accuracy, data points at very high K^2 values will be required. In our range of K^2 values, the least-squares fit resulted in a little smaller $(D_3 - D_1)/D_0$ and Θ values (see the first line in Table I). On the other hand, if both D_0 and Θ values are not given, the three-parameter fit will encounter a difficulty. The data points at low K^2 values will be fitted to

$$F_3(k) \equiv \bar{\Gamma}/K^2 = D_0 - [(D_3 - D_1)/3 - (L^2/12)\Theta/2](KL)^2/45 \quad (22)$$

The data points at high K^2 values will be fitted to

$$F_4(k) \equiv \bar{\Gamma}/K^2 = \{D_0 - (D_3 - D_1)[1/3 - f_2(k)]\} + (L^2/12)\Theta f_1(k) \quad (23)$$

If we had data points at very low K^2 values, the least-squares fit to $F_3(k)$ would determine the D_0 value with a high accuracy. If we had data points at very high K^2 values, the least-squares fit to $F_4(k)$ would determine the Θ value with a high accuracy. When data points are available only in a limited range of K^2, the three-parameter fit does not give accurate results (see the last line in Table I).

As seen from the dashed line in Figure 3, the analysis for a given D_0 value resulted in a little negative deviations at high K^2 values. If we had data points extending to higher K^2 values as in the case of Wilcoxon and Schurr, we would have a little larger value for $(D_3 - D_1)/D_0$ and Θ even in that analysis. The given value of $\Theta = 295$ s^{-1} in the fourth line in Table I came from the result in the first line. Due to similar dependence on K^2 of $f_1(k)$ and $[1/3 - f_2(k)]$ and the limited range of observed points, the reverse analysis did not give the same value for $(D_3 - D_1)/D_0$ (compare the first and the fourth lines in Table I).

From the discussion given above, we can ignore the results in the fifth line in Table I. Also, we leave the results in the fourth line untouched. For other results, however, we have no definite criterion for selecting them. The $(D_3 - D_1)/D_0$ values in the first three lines will have an equal weight. Thus we assume $(D_3 - D_1)/D_0 = (0.412 + 0.500 + 0.510)/3 = 0.474 \pm 0.100$. From the same reason, we assume $\Theta = (295 + 320 + 320)/3 = (312 \pm 30)$ s^{-1}. Using the observed values of $D_0 = (4.29 \pm 0.10) \times 10^{-8}$ cm²/s and $(D_3 - D_1)/D_0 = 0.474 \pm 0.100$, we have $D_1 = (3.61 \pm 0.14) \times 10^{-8}$ cm²/s and $D_3 = (5.64 \pm 0.29) \times 10^{-8}$ cm²/s. These are listed in Table II. We also computed these values by use of formulas of Broersma[28] and Tirado and Garcia de la Torre[14] for $L = 300$ nm and $d = 18$ nm (Table II). The deviation of our values from Broersma's predictions are 2SD (SD = standard deviation) in D_0, 0.4SD in Θ, 1.7SD in $(D_3 - D_1)/D_0$, 2.3SD in D_3, and 0.4SD in D_1. The most significant deviation is in D_3, and due to this, large deviations appear in D_0 and $(D_3 - D_1)/D_0$. On the other hand, deviations of our values from predictions of Tirado and Garcia de la Torre are 2.4SD in D_0, 0.1SD in Θ, 0.8SD in $(D_3 - D_1)/D_0$, 0.28SD in D_3, and 2.3SD in D_1. The most significant deviation in this case is in D_1, and due to this, a large deviation appears in D_0. *If D_3 of Tirado and Garcia de la Torre and D_1 of Broersma were adopted*, our experimental results would be in good agreement with the theoretical predictions, i.e., 0.6SD in D_0 and 0.0SD in $(D_3 - D_1)/D_0$. Our results favor theoretical predictions of high D_3 and low D_1 values.

The theoretical predictions of Tirado and Garcia de la Torre appear to be in good agreement with friction factor measurements performed on macroscopic cylinders. Their formulation raised Θ by 5.7% (from Broersma's), D_1 by 7.1%, and D_3 by 16%. If the experimental D_1 value were reduced to some extent due to unknown factor(s) such as electrolyte friction,[11] a simple increase of only the D_1 value by 2SD ($=0.28 \times 10^{-8}$ cm²/s) would result in simultaneous match of both D_0 and $(D_3 - D_1)/D_0$ with theoretical predictions. Concerning this point, Wilcoxon and Schurr say that their experimental data argue strongly that D_0 and $(D_3 - D_1)/D_0$ cannot both simultaneously match the theoretical predictions. As noted before, however, the correction of $D_{app}(K)$ in their analysis may cause ambiguity in the value of $(D_3 - D_1)/D_0$.

If the literature value having the smallest SD up to now,[15] $\Theta = 318 \pm 3$ s^{-1}, were assumed to hold in our system, we have to conclude that only the D_1 value in our system (and also Wilcoxon and Schurr's) would be affected by some interaction. To discriminate whether the experimental D_1 is too small or the theoretical D_1 is too large, more accurate experimental work is necessary also on other rigid rod systems.

Conclusions

We have measured the spectrum of light quasi-elastically scattered from the suspensions of tobacco mosaic virus and

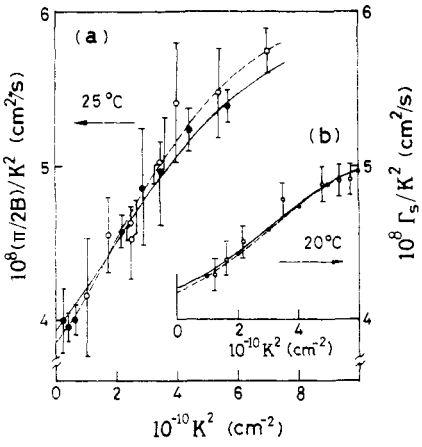

Figure 11. Reanalysis of previous experimental data. (a) The $(\pi/2B)/K^2$ vs. K^2 relationship at 25 °C (from ref 9): (—) reanalyzed result for Θ = 420 s^{-1}; (---) reanalyzed result by a three-parameter fit (see text). Experimental points (○ and ●) are for 0.2 and 0.4 mg/mL TMV suspensions in a 10^{-3} M EDTA buffer (pH 7.5). (b) The Γ_s/K^2 vs. K^2 relationship at 20 °C (from ref 17). The length of the error bar shows a ±3% standard deviation mentioned in ref 17. (○) Average of three results for independently prepared TMV samples; (●) simulated results for $D_0 = 4.2 \times 10^{-8}$ cm^2/s, Θ = 320 s^{-1}, and $(D_3 - D_1)/D_0 = 0.3$; (—) the best fit curve to the experimental points; (---) best fit curve to simulated result (see text). Concentrations, 0.03–0.1 mg/mL; ionic strength, 10^{-3} M EDTA to 0.05 M NaCl.

discussed the effect of anisotropy in translational diffusion on the correlation function. Diffusion coefficients D_0 and Θ of TMV were obtained by the analyses of both the cumulant method and the two-exponential fit against K^2. The experimentally obtained value of D_0 corrected to 20 °C in water is considerably larger than those of previous dynamic light scattering studies and is in good agreement with those of Wilcoxon and Schurr from both light scattering and sedimentation.[11] This value lies in between Broersma's and Garcia de la Torre's predictions. The anisotropy ratio of the translational diffusion coefficient, $(D_3 - D_1)/D_0$, is a little larger than those of Wilcoxon and Schurr and of the theoretical prediction. The present result confirmed the observation of Wilcoxon and Schurr about the strong effect of anisotropy in translational diffusion on the dynamic structure factor for a long rod. The detailed examination of correlation functions against K^2 was carried out with the aid of the theoretical formulation which takes account of the effect of anisotropy. The correlation functions based on the theory well reproduced the measured correlation functions in both time and K^2 dependences. This again confirms that the effect of anisotropy in translational diffusion affects the correlation functions over the whole range of time at large K^2. The validity of theoretical expressions for $g^{(1)}(\tau)$[21,23] is now experimentally confirmed.

Acknowledgment. We thank Dr. S. Kubo of the Central Research Institute, the Japan Tobacco and Salt Public Corp., for his generous gift of tobacco mosaic virus samples, Professor F. Kitahara of the Science University of Tokyo for permission to use the Ar ion laser, and Drs. Y. Yano-Toyoshima and T. Miki-Noumura of Ochanomizu University for assisting in electron microscopy. We also thank the Nishina Memorial Foundation.

Appendix A. Reconsideration of Some Previous Studies

We briefly reconsider some previous studies in light of the new result shown in the text.

Let $S(K,\omega)$ and $S_0(K,\omega)$ be, respectively, the homodyne power spectra for nonzero and zero anisotropy ratios, $(D_3 - D_1)/D_0$. The difference $C(K,\omega) \equiv S(K,\omega) - S_0(K,\omega)$ gives the contribution from anisotropy. By using Pecora's $S_n(k)$'s in eq 10 and the D_0 value determined at low K^2 values, Fujime[8] tried to determine the Θ value based on $S_0(K,\omega)$. In that process, if the low-frequency (or main) portion of the experimental spectra at $\theta \geq 140°$ were fit to $S_0(K,\omega)$ with the Θ value determined at $90° \leq \theta \leq 120°$, a discrepancy appeared in the high-frequency (or wing) portion. Moreover, the best fit D_0 and Θ values became smaller as the scattering angle was increased. *This difficulty can be understood from $P_0 > S_0$ and $P_2 < S_2$.* The experimentally extracted $C(K,\omega)$ at the scattering angles of 160° and 180° (both correspond to $K^2 \simeq 7 \times 10^{10}$ cm^{-2}) behaved in a very close manner with the numerical result of Maeda and Saito[16] both in size (if $(D_3 - D_1)/D_0 \simeq 0.6$ was assumed) and in frequency dependence. From this, Fujime suggested the importance of the coupling effect.

Schaefer et al.[9] questioned a large effect of anisotropy from their elaborate study for 0.2 and 0.4 mg/mL TMV suspensions. They derived

$$(\pi/2B)/K^2 = \bar{D}[1 + K^2(\mu I_\mu + \rho I_\rho)] \qquad \text{(A1)}$$

of which the right-hand side is easily rewritten in our notation (see Appendix B in ref 23) as $D_0 - (D_3 - D_1)[^1/_3 - f_2(k)] + (L^2/12)\Theta f_1(k)$. The far wings of the normalized homodyne power spectrum can be asymptotically written as $S(K,\omega) = (A + B\omega^2)^{-1}$. The quantity B is related to the first cumulant of the correlation function;[4] i.e., $\pi/2B = \bar{\Gamma}$. Thus, eq A1 is the same as eq 18. Then why did Schaefer et al. not obtain a large anisotropy ratio? At $K^2 = 7 \times 10^{10}$ cm^{-2}, their data show $(\pi/2B)/K^2 - \bar{D} \simeq 1.8 \times 10^{-8}$ cm^2/s, *which is two times larger than our value (and also Wilcoxon and Schurr's value)*; i.e., $\bar{\Gamma}/K^2$ [or $(2\tau_c K^2)^{-1}$] $- D_0 \simeq 0.9 \times 10^{-8}$ cm^2/s at 25 °C. The large values of $(\pi/2B)/K^2 - \bar{D}$ resulted in a negligibly small value of the anisotropy ratio for their "given" value of Θ = 420 s^{-1} at 25 °C. We reanalyzed their data with eq 11. The three-parameter fit with the weight inversely proportional to the length of the error bar yielded $D_0 = (3.84 \pm 0.09) \times 10^{-8}$ cm^2/s and $\Theta = 447 \pm 140$ s^{-1} (both at 25 °C) and $(D_3 - D_1)/D_0 = 0.117 \pm 0.564$. The Θ value of 447 s^{-1} at 25 °C (or 390 s^{-1} at 20 °C) seems to be large compared with other results (although the largest value in the literature is Θ = 390 s^{-1} at 20 °C[8]). For a given value of Θ = 420 s^{-1} at 25 °C as they assumed (or 366 s^{-1} at 20 °C, which is the upper bound of recent values), the least-squares fit yielded $D_0 = (3.91 \pm 0.07) \times 10^{-8}$ cm^2/s and $(D_3 - D_1)/D_0 = 0.137 \pm 0.072$. This value of the anisotropy ratio is about one-third of our value, but 5.5 times larger than their value, 0.025. Figure 11a shows how these values reproduce their data. Their large values of $(\pi/2B)/K^2 - \bar{D}$ might come from difficulties in deducing precise B values from the far wings of normalized power spectra at large K^2 values.

Hartford[17] gave Γ_s/K^2 values from the best single Lorentzian fit for 0.03–0.1 mg/mL TMV suspensions over the K^2 range $(1.24–5.74) \times 10^{10}$ cm^{-2}. At the highest K^2 value, his data show $\Gamma_s/K^2 - D_0 \simeq 0.7 \times 10^{-8}$ cm^2/s, which is very close to our value. *By applying eq 11 to the Γ_s/K^2 vs. K^2 relationship,* $D_0 = (4.21 \pm 0.07) \times 10^{-8}$ cm^2/s at 20 °C and $(D_3 - D_1)/D_0 = 0.52 \pm 0.07$ were obtained for a given value of Θ = 320 s^{-1}, and $(D_3 - D_1)/D_0 = 0.47 \pm 0.13$ and Θ = 310 ± 27 s^{-1} for a given value of $D_0 = 4.2 \times 10^{-8}$ cm^2/s (Figure 11b). Because eq 11 has been derived for $\bar{\Gamma}/K^2$ and not Γ_s/K^2, some correction to the result is required as in the case of Wilcoxon and Schurr. By putting $D_0 = 4.2 \times 10^{-8}$ cm^2/s, Θ = 320 s^{-1}, and $(D_3 - D_1)/D_0 = 0.2–0.5$, homodyne power spectra were simulated by use of eq 12b. The Γ_s/K^2 vs. K^2 relationship from spectra for $(D_3 - D_1)/D_0 = 0.3$ resembled his result (solid circles in Figure

11b). The simulated result was analyzed by eq 11 and $D_0 = (4.18 \pm 0.01) \times 10^{-8}$ cm^2/s and $(D_3 - D_1)/D_0 = 0.48 \pm 0.02$ were obtained for a given value of $\Theta = 320$ s^{-1}. From the above results, his experimental data are considered to suggest $(D_3 - D_1)/D_0 \simeq 0.3$ at least.

If previous results were reanalyzed by the new method, most of them would show nonzero anisotropy ratios. In all cases,[8,9,17] however, the incident beam from a low-power He–Ne laser and an analog spectral method prevent us from obtaining a very quantitative result on anisotropy.

Appendix B. Eigenvalues of the Matrix M in Eq 3

With the eigenvalue and the column eigenvector of **M** as $\lambda_p = \lambda_p^{(0)} + \epsilon\lambda_p^{(1)} + \epsilon^2\lambda_p^{(2)} + \ldots$ and $\mathbf{U}_p = \mathbf{U}_p^{(0)} + \epsilon\mathbf{U}_p^{(1)} + \ldots$, respectively, we have

$$\lambda_p^{(0)} = p(p+1) + \mu^2 L_0(p)$$

and

$$\mathbf{U}_p^{(0)} = [0, \ldots, 0, 1, 0, \ldots, 0]^t \qquad \text{(B1)}^{23}$$

Define $H_{k,p} = [\mathbf{U}_k^{(0)}]^t \mathbf{M}^{(1)} \mathbf{U}_p^{(0)}$. We have only four kinds of $H_{k,p}$'s:

$$H_{p,p-2} = \mu^2 L_1(p)$$

$$H_{p,p+2} = \mu^2 L_2(p)$$

$$H_{p-2,p} = \mu^2 L_2(p-2)$$

and

$$H_{p+2,p} = \mu^2 L_1(p+2) \qquad \text{(B2)}^{23}$$

Since $H_{p,p} = 0$, we have $\lambda_p^{(1)} = 0$. The $\lambda_p^{(2)}$ is given by a formula

$$\lambda_p^{(2)} = \sum_{m \neq p} H_{p,m} H_{m,p} / [\lambda_p^{(0)} - \lambda_m^{(0)}] = [A_{p-2}(\mu^2) - A_p(\mu^2)]\mu^4 \qquad \text{(B3)}$$

where

$$A_p(\mu^2) = [(p+1)^2(p+2)^2(2p-1)(2p+7)]/\{2(2p+1) \times (2p+3)(2p+5)[(2p-1)(2p+3)^2(2p+7) - 2\mu^2]\} \qquad \text{(B4)}$$

These results were used to express Γ_0 and Γ_2 in eq 12c,d and to draw the dotted lines in Figure 8.

References and Notes

(1) Berne, B.; Pecora, R. "Dynamic Light Scattering"; Interscience: New York, 1975.
(2) Chu, B. "Laser Light Scattering"; Academic Press: New York, 1974.
(3) de Gennes, P.-G. "Scaling Concepts in Polymer Physics"; Cornell University Press: London, 1979.
(4) Maeda, T.; Fujime, S. *Macromolecules* **1981**, *14*, 809.
(5) Dubin, S. B.; Lunacek, J. H.; Benedek, G. B. *Proc. Natl. Acad. Sci. U.S.A.* **1967**, *57*, 1164.
(6) Cummins, H. Z.; Carlson, F. D.; Herbert, T. J.; Woods, G. *Biophys. J.* **1969**, *9*, 518.
(7) Wada, A.; Suda, N.; Tsuda, T.; Soda, K. *J. Chem. Phys.* **1969**, *50*, 31.
(8) Fujime, S. *J. Phys. Soc. Jpn.* **1970**, *29*, 416.
(9) Schaefer, W. D.; Benedek, G. B.; Schofield, P.; Bradford, E. *J. Chem. Phys.* **1971**, *55*, 3884.
(10) Loh, E.; Ralston, E.; Schumaker, V. N. *Biopolymers* **1979**, *18*, 2549.
(11) Wilcoxon, J.; Schurr, J. M. *Biopolymers* **1983**, *22*, 849.
(12) Boedtker, H.; Simmons, N. *J. Am. Chem. Soc.* **1958**, *80*, 2550.
(13) Broersma, S. J. *J. Chem. Phys.* **1960**, *32*, 1626.
(14) Tirado, M.; Garcia de la Torre, J. *J. Chem. Phys.* **1979**, *71*, 2581.
(15) Quoted in: Newman, J.; Swinney, H. L. *Biopolymers* **1976**, *15*, 301.
(16) Maeda, H.; Saito, N. *J. Phys. Soc. Jpn.* **1969**, *27*, 984.
(17) Hartford, S. L. Ph.D. Thesis, University of Illinois, 1975.
(18) Rallison, J. M.; Leal, L. G. *J. Chem. Phys.* **1981**, *74*, 4819.
(19) Wada, A.; Ford, N. C., Jr.; Karasz, F. E. *J. Chem. Phys.* **1971**, *55*, 1798.
(20) Pecora, R. *J. Chem. Phys.* **1968**, *49*, 4126.
(21) Gierke, T. D. Ph.D. Thesis, University of Illinois, 1973.
(22) Loh, E. *Biopolymers* **1979**, *18*, 2569.
(23) Maeda, T.; Fujime, S. *Macromolecules* **1984**, *17*, 1157, where D_3 in eq 38a and $(2n-5)$ in eq B2 should read $D_3/3$ and $(2n+5)$, respectively.
(24) C.M.I./A.A.B. Description of Plant Viruses, 1975.
(25) Ohbayashi, K.; Kohno, T.; Utiyama, H. *Phys. Rev. A* **1983**, *27*, 2632.
(26) Koppel, D. E. *J. Chem. Phys.* **1972**, *57*, 4814.
(27) Koene, R. S.; Mandel, M. *Macromolecules* **1983**, *16*, 220.
(28) Broersma's revised equations in ref 15 and in Newman et al. (Newman, J.; Swinney, H. L.; Day, L. A. *J. Mol. Biol.* **1977**, *116*, 593) are used.

Electron Spin Resonance Studies of Ionic Interactions in Sulfonated Polystyrene Ionomers: Manganese(II) Salts

Hirokazu Toriumi and R. A. Weiss*

Institute of Materials Science, University of Connecticut, Storrs, Connecticut 06268

Harry A. Frank

Department of Chemistry, University of Connecticut, Storrs, Connecticut 06268.

Received December 5, 1983

ABSTRACT: Ionic interactions in sulfonated polystyrene manganese(II) salts were studied by electron spin resonance spectroscopy. It is shown by comparison with earlier small-angle X-ray scattering observations that the aggregation of ionic groups in unheated samples develops from isolated ions through multiplets into clusters as the ionic group concentration is increased, while in samples once heated above their glass transition temperature multiplets predominate. The formation and decomposition of higher order ionic aggregates are discussed in terms of a competition between attractive interactions of ionic groups and elastic constraints associated with the segmental motions of backbone chains. The observed ESR spectra are satisfactorily reproduced by a combination of two reference spectra representing an isolated Mn^{2+} ion and coupled Mn^{2+}---Mn^{2+} ions, from which the proportion of ions participating in the aggregation may be estimated.

Introduction

Self-organization or clustering of ionic groups influences the morphology and physical properties of ion-containing organic polymers (ionomers).[1] The most striking observation in the study of ionomers is a small-angle X-ray scattering (SAXS) peak that commonly appears for all ionomers in the salt form. The scattering entity responsible for this peak is believed to be aggregated ionic groups

0024-9297/84/2217-2104$01.50/0 © 1984 American Chemical Society